

Supporting Information for
Unraveling cholesterol catabolism in *Mycobacterium tuberculosis*: the ChsE4-ChsE5 $\alpha_2\beta_2$ acyl-CoA dehydrogenase initiates β -oxidation of 3-oxo-cholest-4-en-26-oyl CoA

Meng Yang,¹ Rui Lu,¹ Kip E. Guja,² Matthew F. Wipperman,¹ Johnna R. St. Clair,³ Amber C. Bonds,² Miguel Garcia-Diaz,² and Nicole S. Sampson^{1,*}

¹Department of Chemistry, Stony Brook University, Stony Brook, NY 11794-3400

²Department of Pharmacological Sciences, Stony Brook University, Stony Brook, NY 11794-8651

³Biochemistry and Structural Biology Graduate Program, Stony Brook University, Stony Brook, NY 11794-5215

Table of Contents

Table S1. Gene constructs used in this study	S3
Figure S1. Analytical ultracentrifugation (AUC) sedimentation equilibrium analysis	S4
Figure S2. Purification of the ChsE4 _{E247A} -ChsE5 mutant and its catalytic activity with 3-OCS-CoA; analysis of product formation catalyzed by ChsE4-ChsE5 with 3-OCS-CoA as the substrate	S5
Figure S3. The dehydrogenation of 3-OCO-CoA	S6
Figure S4. Small Angle X-ray Scattering (SAXS) generates a tetrameric envelope for solution state ChsE4-ChsE5	S7
Figure S5. The FAD cofactor is reduced upon X-ray irradiation	S8
Figure S6. The three acyl-CoA dehydrogenase (ACAD) domains of ChsE4 and ChsE5	S9
¹ H, ¹³ C NMR spectra of compounds 3 , 4 , 5 , 6 , 7 , 8 , 9 , 10 , 11	S10-S27

Table S1. Gene constructs used in this study.

construct	vector	gene	gene name	<i>His</i> ₆ tag	selection	source or ref
<i>p26N/27</i>	<i>pET28b</i>	<i>Rv3504/Rv3505</i>	<i>ChsE4/ChsE5</i>	<i>N-terminal</i>	<i>Kan</i>	<i>I</i>
<i>p26N</i>	<i>pET28b</i>	<i>Rv3504</i>	<i>ChsE4</i>	<i>N-terminal</i>	<i>Kan</i>	<i>This work</i>
<i>p27</i>	<i>pET20b</i>	<i>Rv3505</i>	<i>ChsE5</i>	<i>no tag</i>	<i>Amp</i>	<i>This work</i>
<i>p34N</i>	<i>pET28b</i>	<i>Rv3573c</i>	<i>ChsE3</i>	<i>N-terminal</i>	<i>Kan</i>	<i>This work</i>
<i>p26N_{E247A}/27</i>	<i>pET28b</i>	<i>Rv3504/Rv3505</i>	<i>ChsE4/ChsE5</i>	<i>N-terminal</i>	<i>Kan</i>	<i>This work</i>

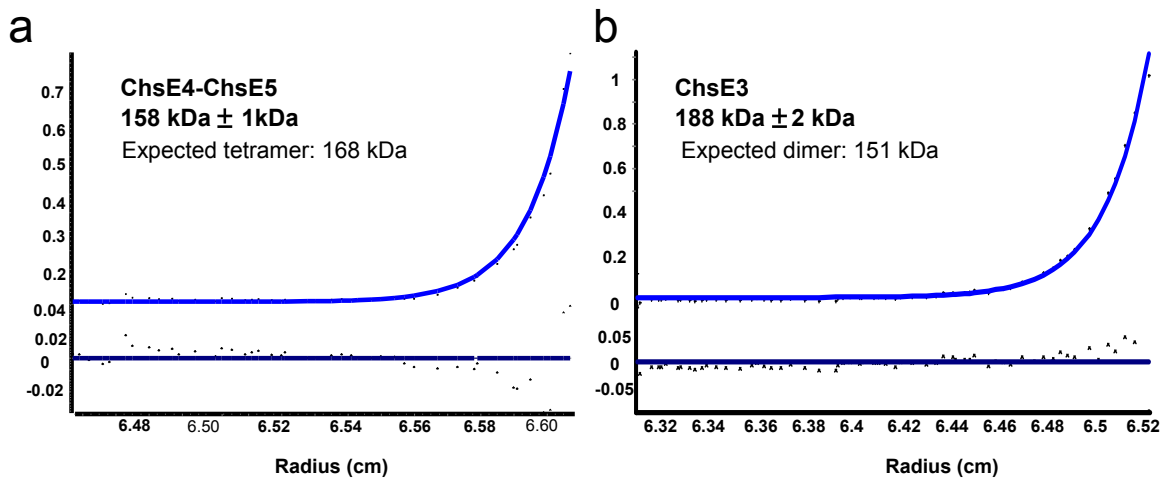


Figure S1. Analytical ultracentrifugation (AUC) sedimentation equilibrium analysis. (a) ChsE4-ChsE5 (5.18 μ M, 2.28 μ M, and 1.08 μ M) and (b) ChsE3 (6.09 μ M, 3.05 μ M, and 1.52 μ M) were centrifuged at speeds of 20k, 25k, and 30k rpm at 20° C in an analytical ultracentrifuge. The solid line (*light blue*) shows the fit of the data to the ideal species model and the residuals of the fit are graphed below the fit (*dark blue*). The best global fit for each protein is shown. Experimentally determined molecular weights are shown for each sample.

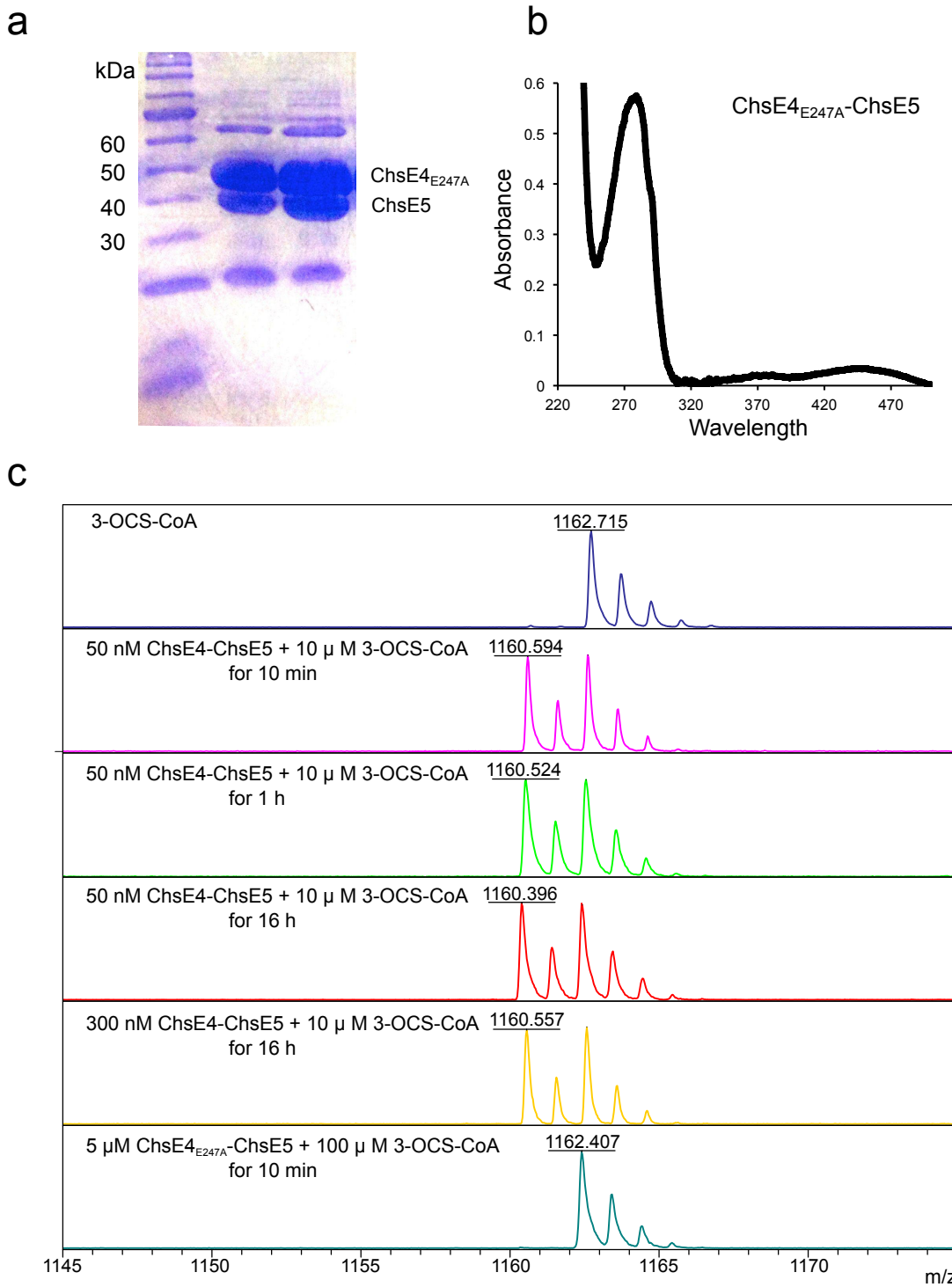


Figure S2. Purification of the ChsE4_{E247A}-ChsE5 mutant and its catalytic activity with 3-OCS-CoA; analysis of product formation catalyzed by ChsE4-ChsE5 with 3-OCS-CoA as the substrate. (a) SDS-PAGE gel analysis of the purified ChsE4_{E247A}-ChsE5 (b) The UV-visible spectrum of the purified ChsE4_{E247A}-ChsE5 showing the characteristic FAD absorbance. (c) Analysis of the product formation of ChsE4-ChsE5 with 3-OCS-CoA diastereomers as a function of time and increased enzyme concentration. The spectra revealed that the percent substrate conversion remained fixed at a 1:1 ratio of product to substrate.

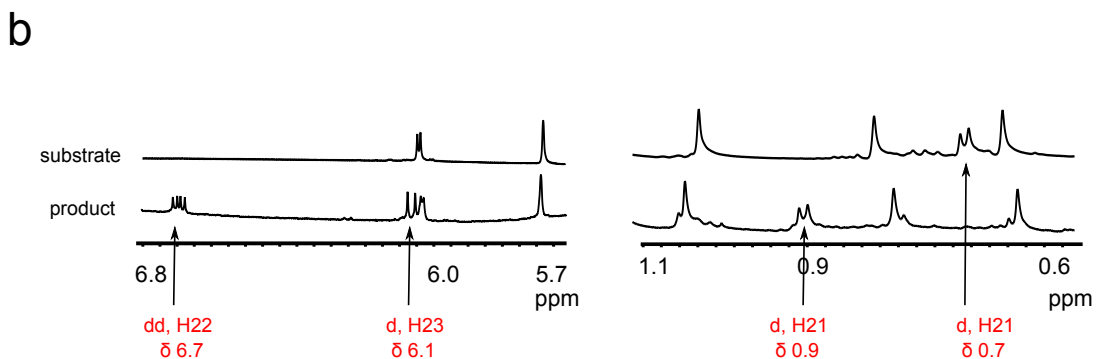
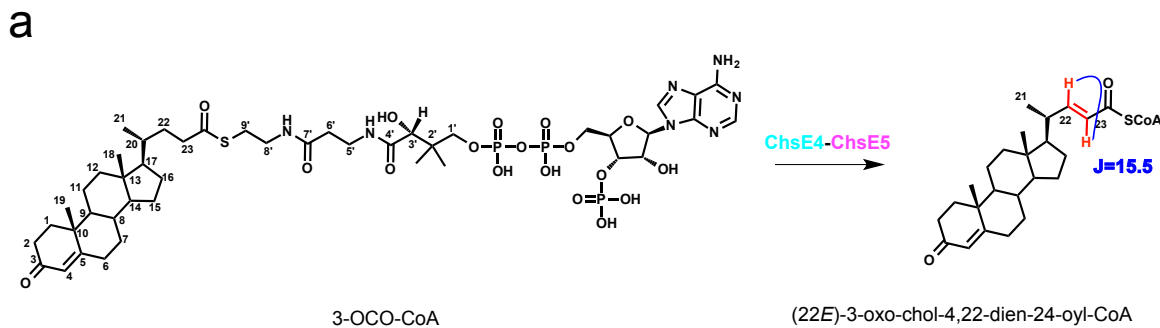


Figure S3. The dehydrogenation of 3-OCO-CoA. (a) ChsE4-ChsE5 catalyzes the formation of (22*E*)-3-oxo-chol-4,22-dien-24-oyl-CoA, (b) as determined by the observed chemical shift and coupling constant. The C22 and C23 olefinic protons appear at 6.7 and 6.1 ppm as doublets in the product spectrum (panel b, left), and the double bond induces a downfield shift of the C20 proton and C21 methyl proton resonances (panel b, right).

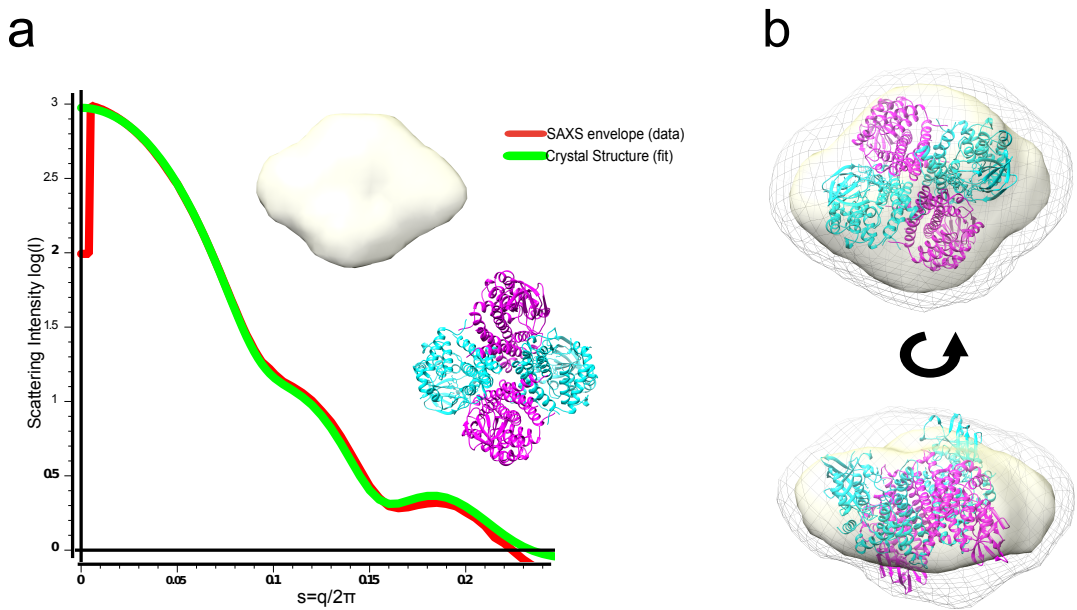
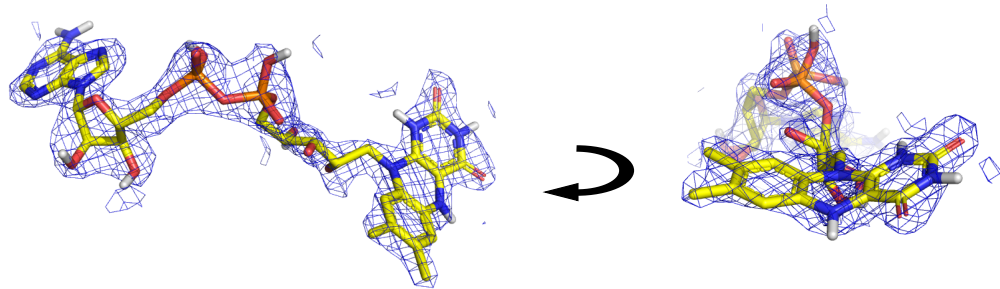


Figure S4. Small Angle X-ray Scattering (SAXS) generates a tetrameric envelope for solution state ChsE4-ChsE5. Small-angle X-ray scattering was used to determine the envelope of the solution state ChsE4-ChsE5 protein complex. (a) The theoretical scattering profile of the ChsE4-ChsE5 crystal structure, defined as scattering intensity (I), versus scattering vector (s) was calculated with CRYSTAL and fit to the experimentally determined scattering profile for ChsE4-ChsE5 in solution, and the Chi-value (the square root of Chi squared) is 2.8. (b) The molecular envelope of solution state ChsE4-ChsE5 was determined from the experimental scattering profile using the ASTAS package. Then the high-resolution crystal structure was subsequently docked into the molecular envelope in Chimera, and the correlation coefficient is 0.90.

a



b

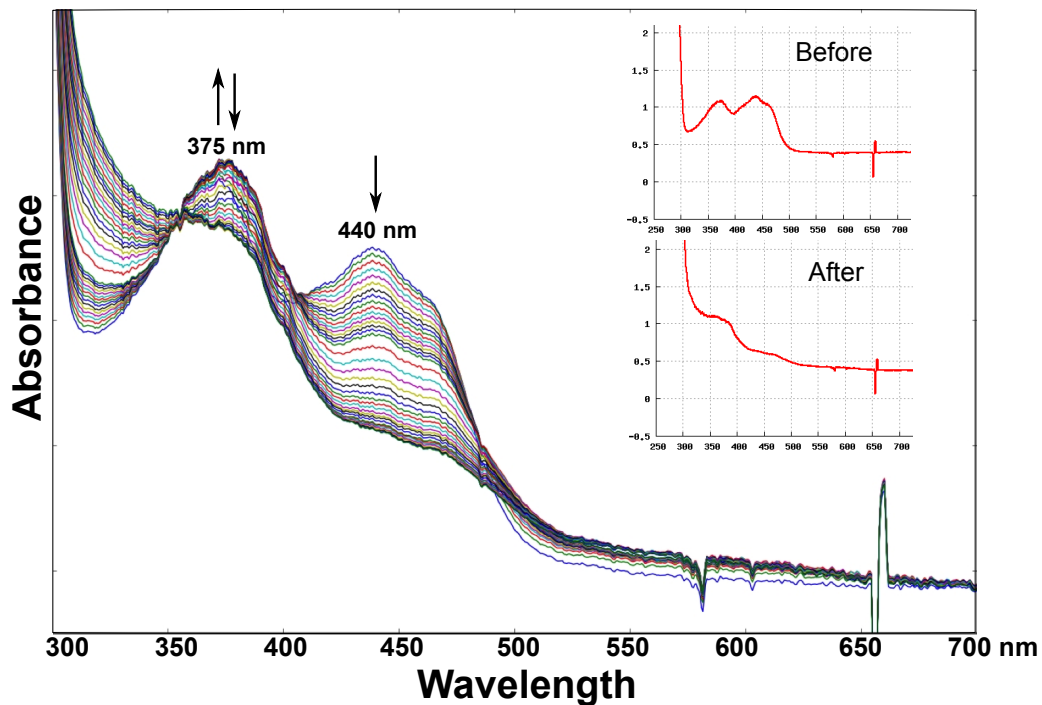


Figure S5. The FAD cofactor is reduced upon X-ray irradiation. To investigate the potential reduction of FAD cofactor during our X-ray diffraction data collection, we collected a full dataset of X-ray diffraction with simultaneous optical spectroscopy as a function of X-ray exposure on beamline X26-C of the NSLS. The optical absorption spectra were collected during the readout of each X-ray diffraction image and an overlay of spectra during the diffraction data collection was constructed. (a) A simulated annealing $F_o - F_c$ omit map for the bound cofactor was calculated to reduce the effects of model bias. The electron density was contoured at 2.5σ and displayed as blue mesh. The polar hydrogens are shown to clearly represent the oxidation state, but they are not present in the deposited coordinates. (b) Correlated absorption spectroscopy data for the ChsE4-ChsE5 crystal were collected as a function of X-ray exposure. The spectra were overlaid and the changes at 440 nm and 375 nm are shown. Inset. two spectra, one at the beginning and one at the end of X-ray exposure, were selected to highlight the change in absorbance.

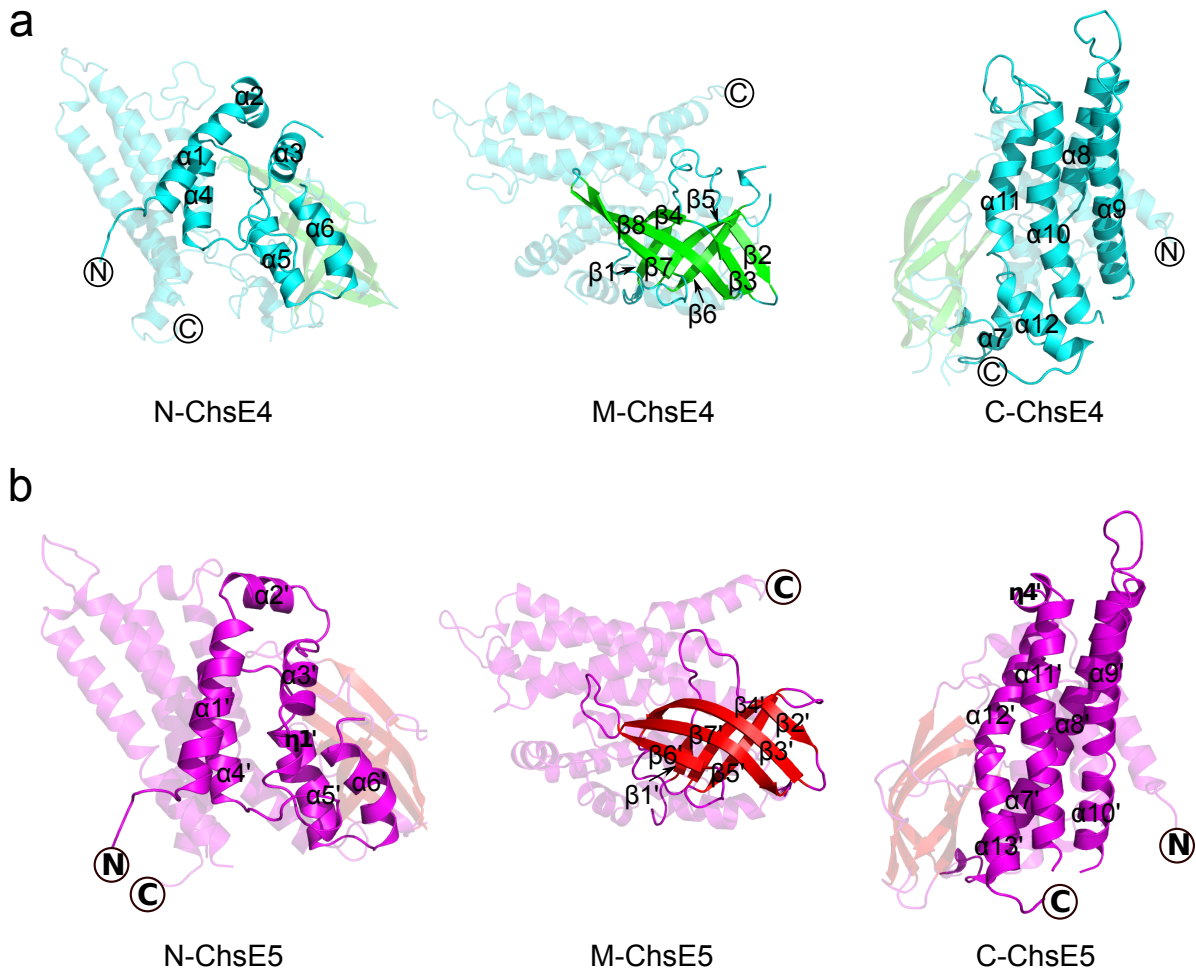
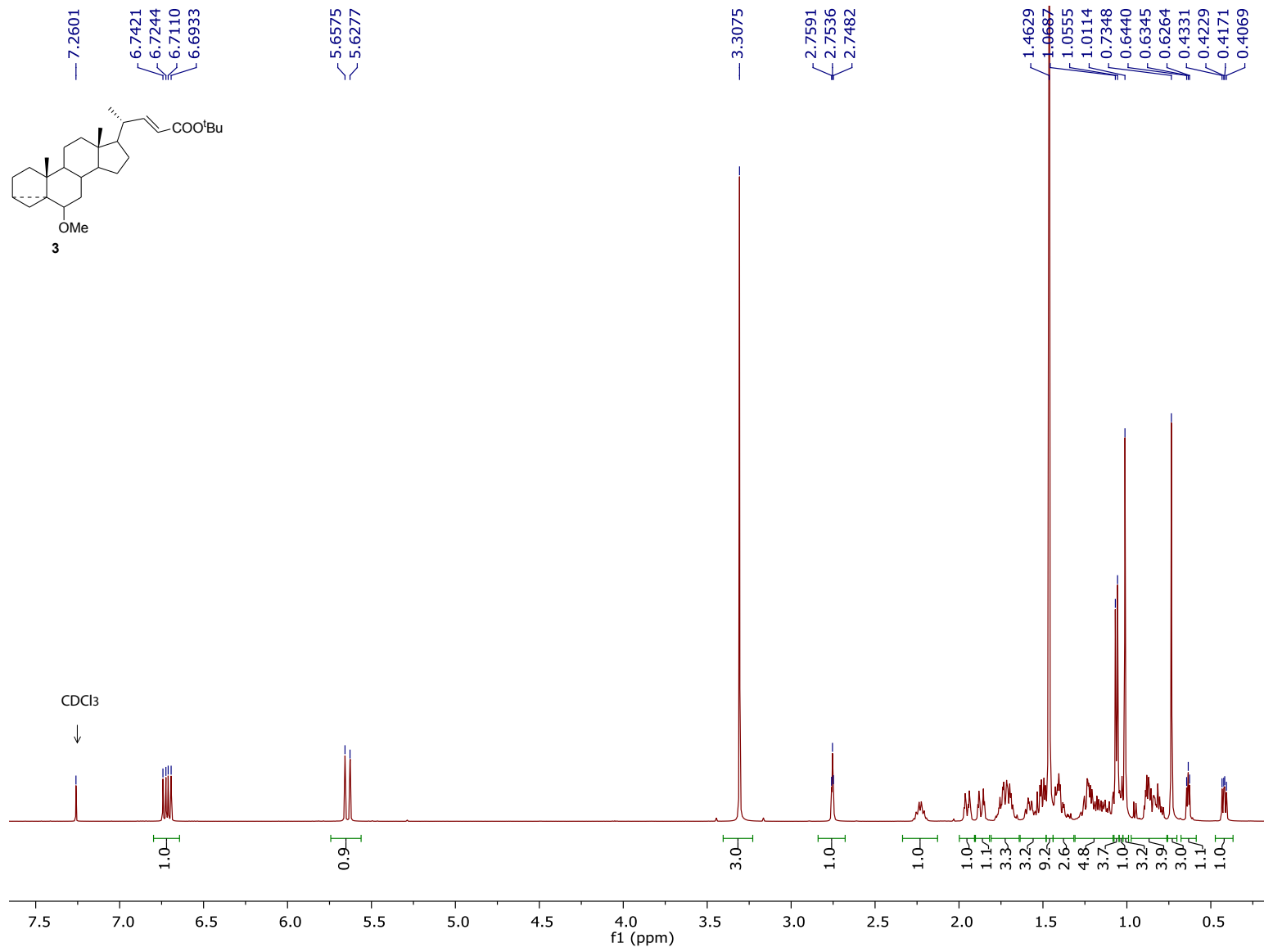
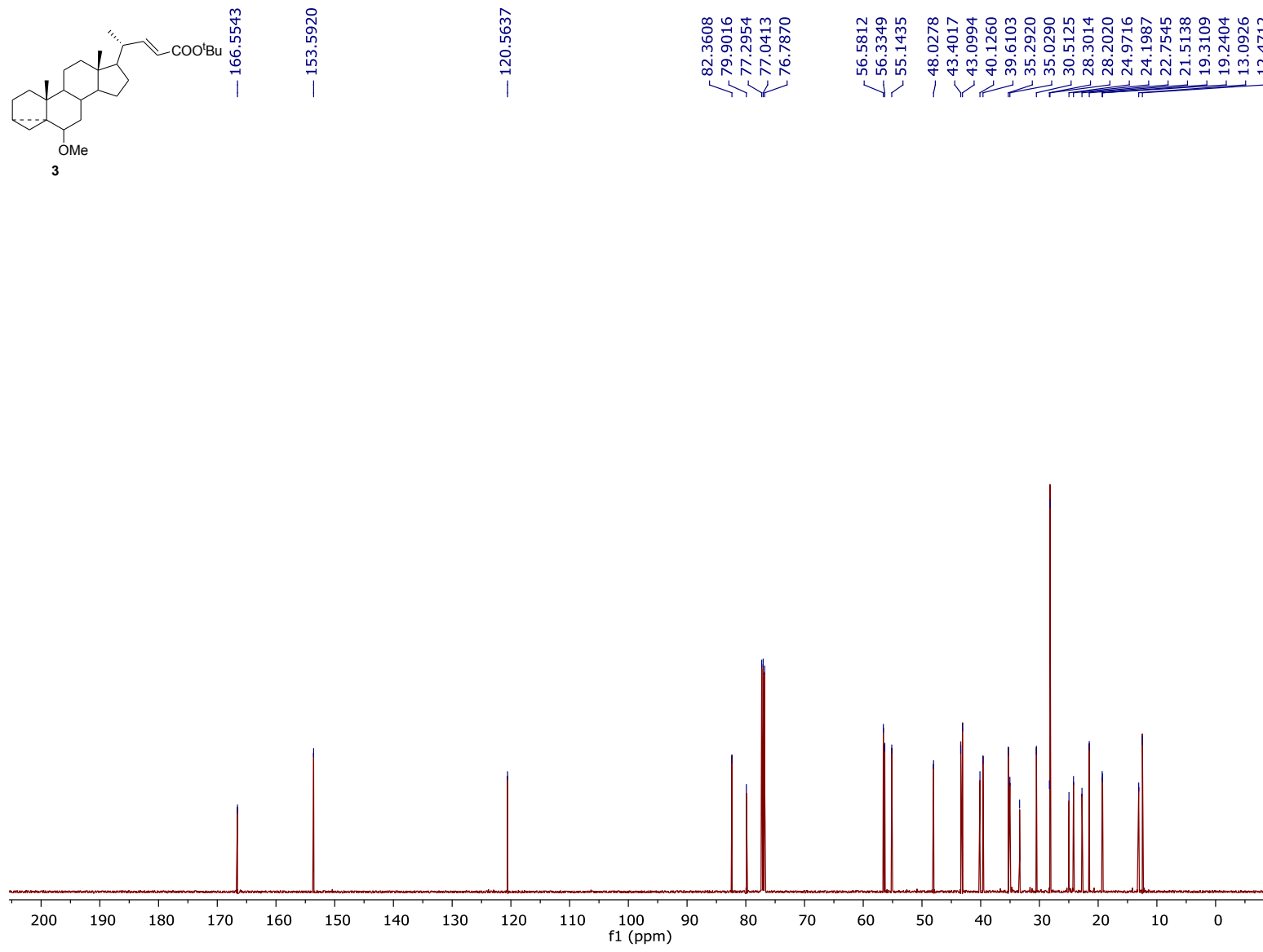
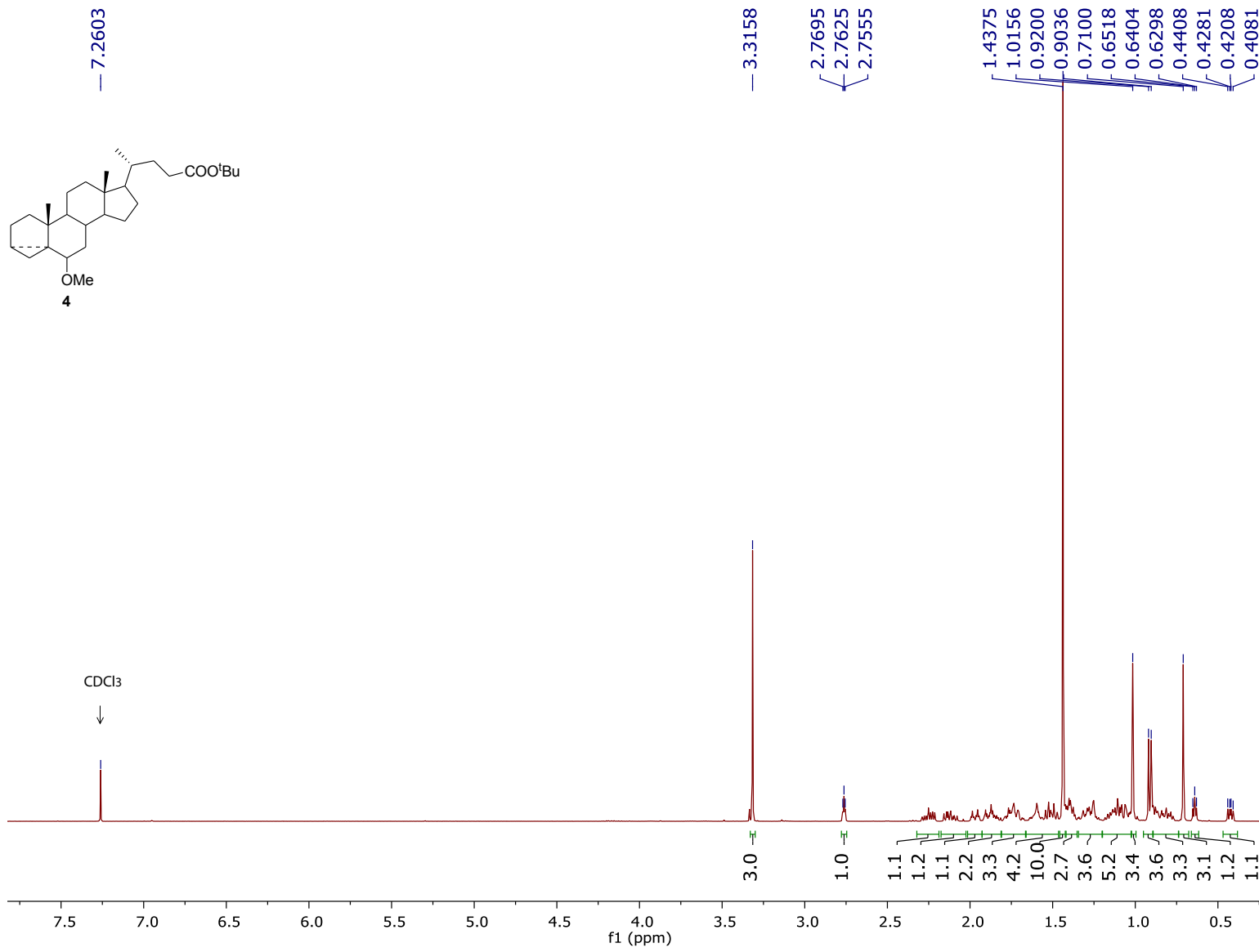
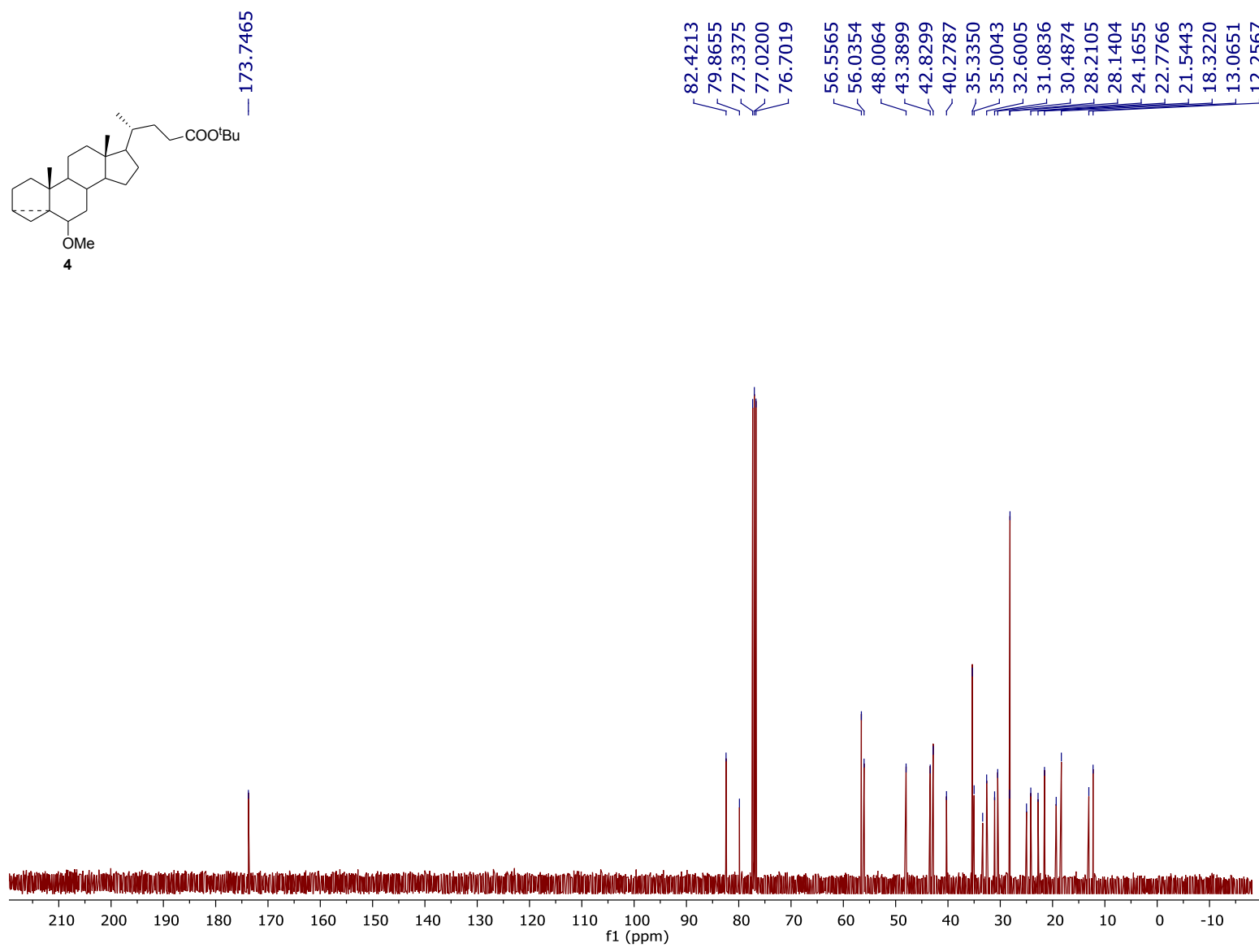


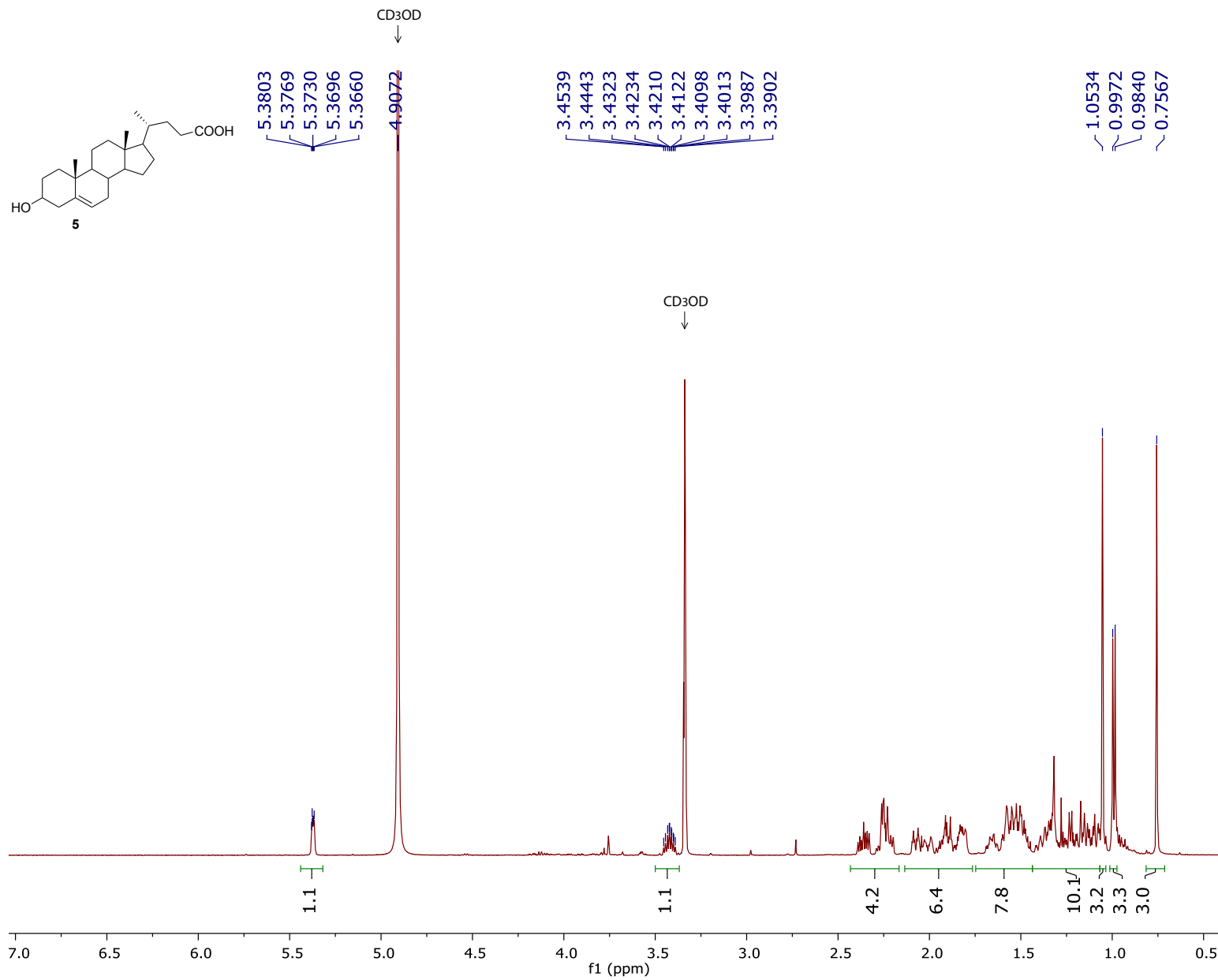
Figure S6. The three acyl-CoA dehydrogenase (ACAD) domains of ChsE4 and ChsE5. (a) ChsE4 and (b) ChsE5 both possess three ACAD domains: N-terminal domain (N-ChsE4; N-ChsE5), Middle domain (M-ChsE4; M-ChsE5), and C-terminal domain (C-ChsE5; C-ChsE5).

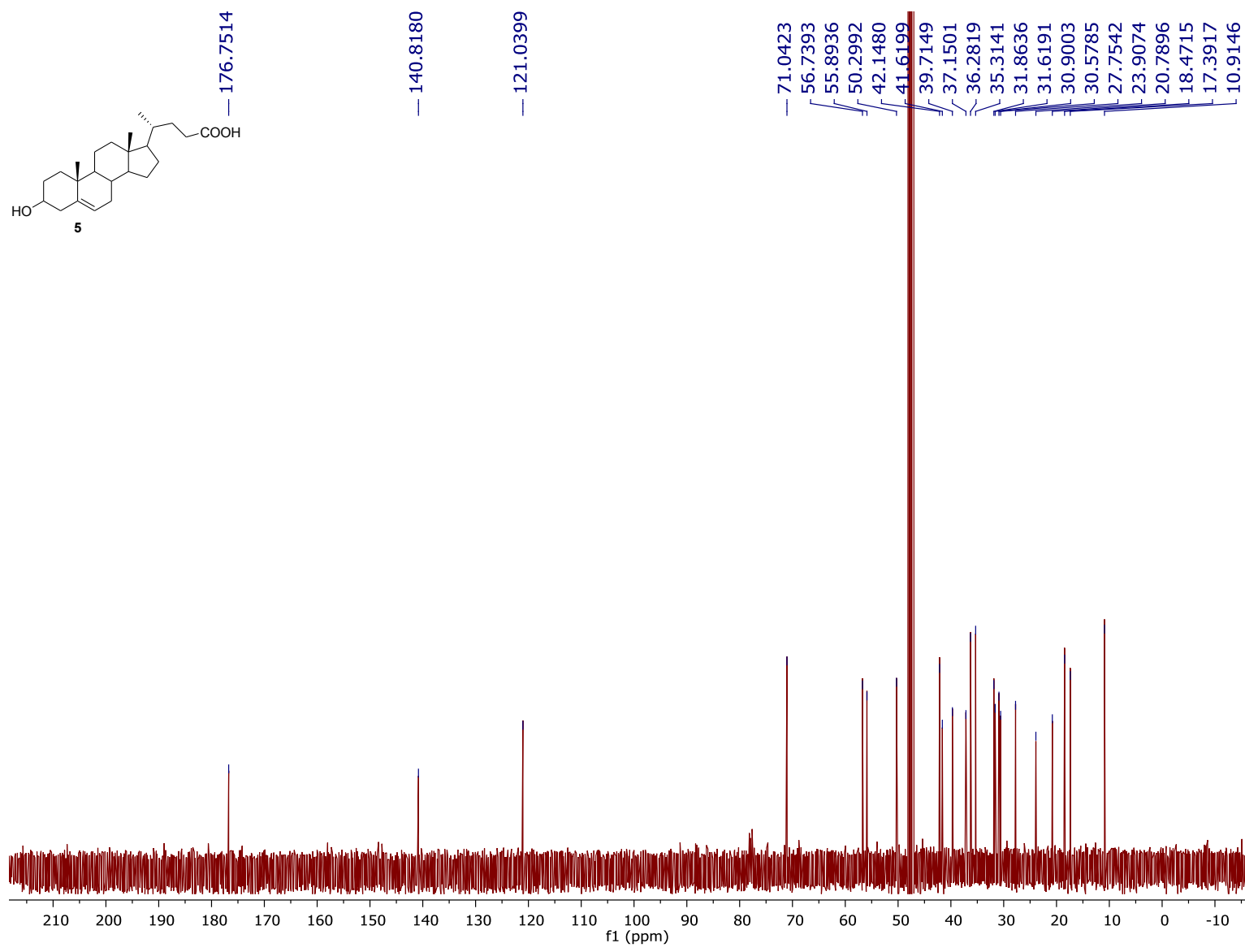


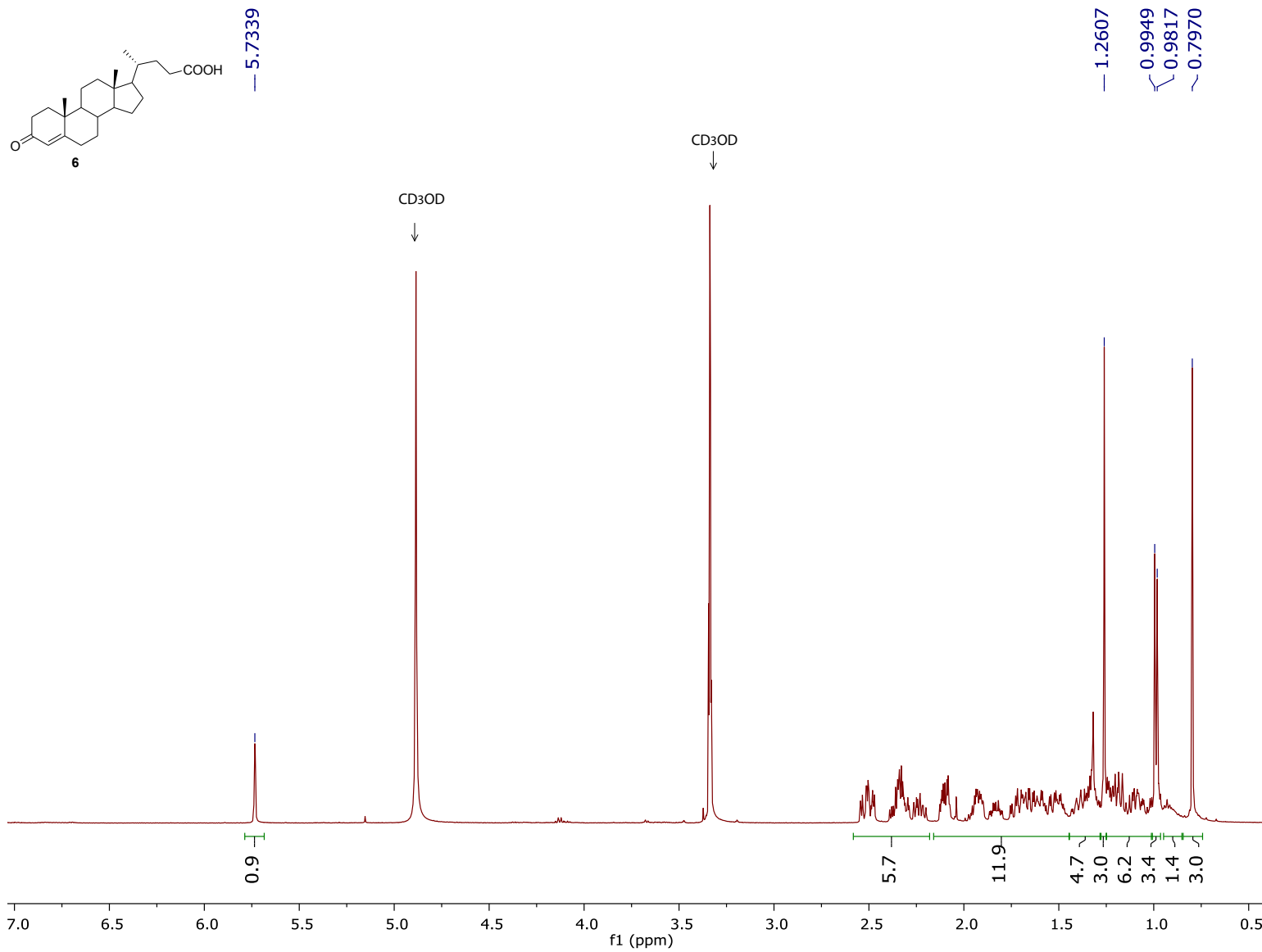


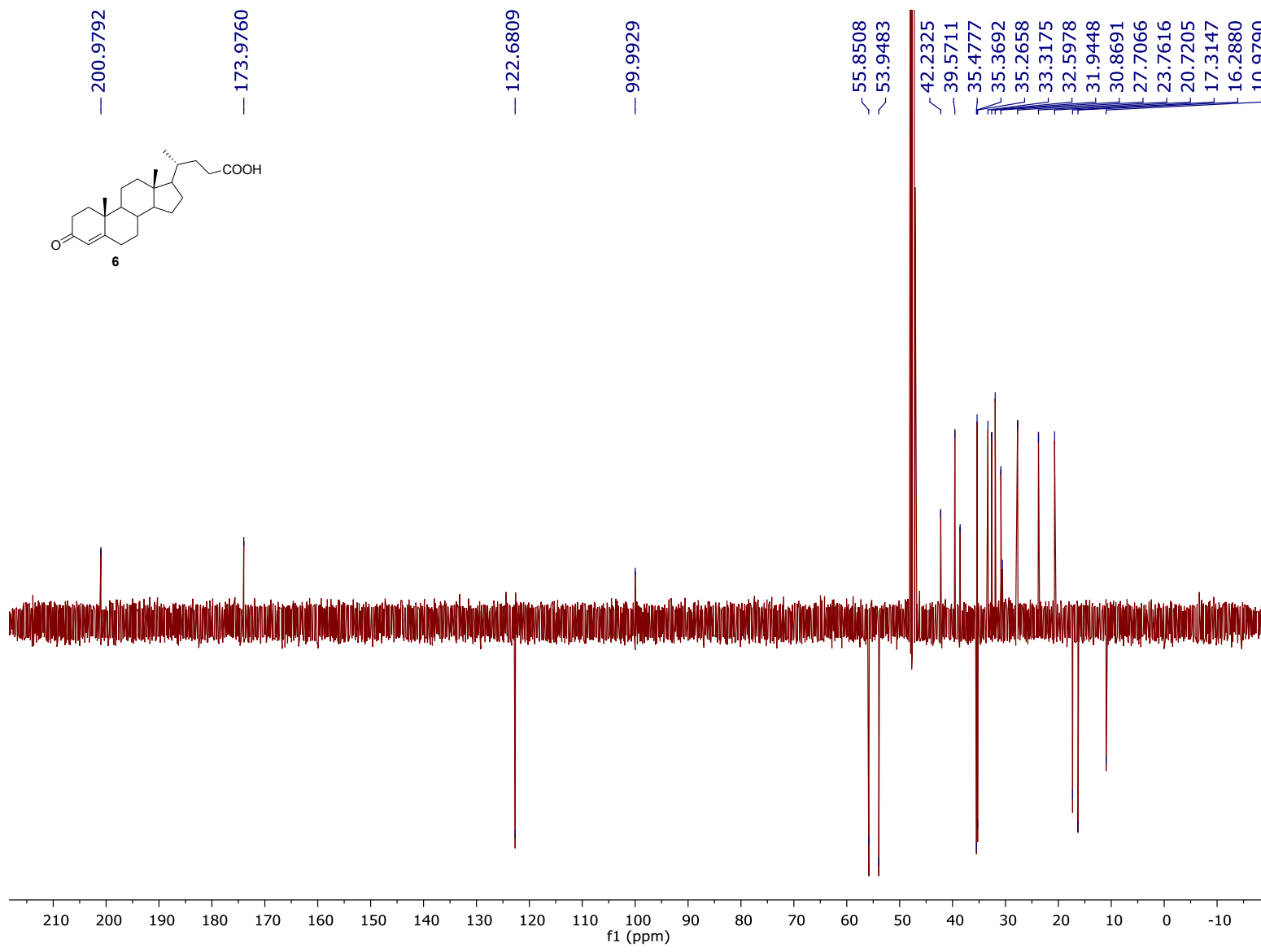


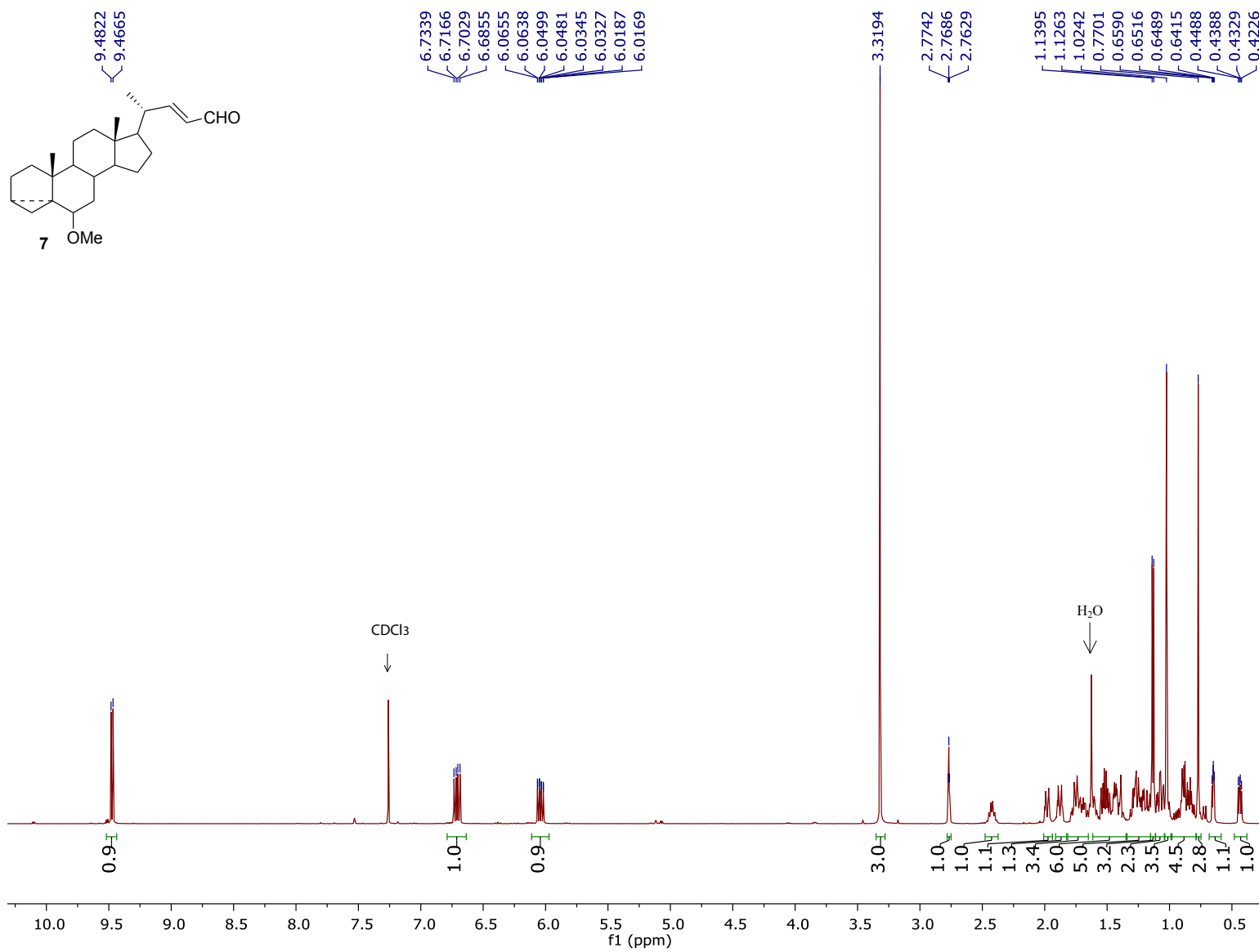


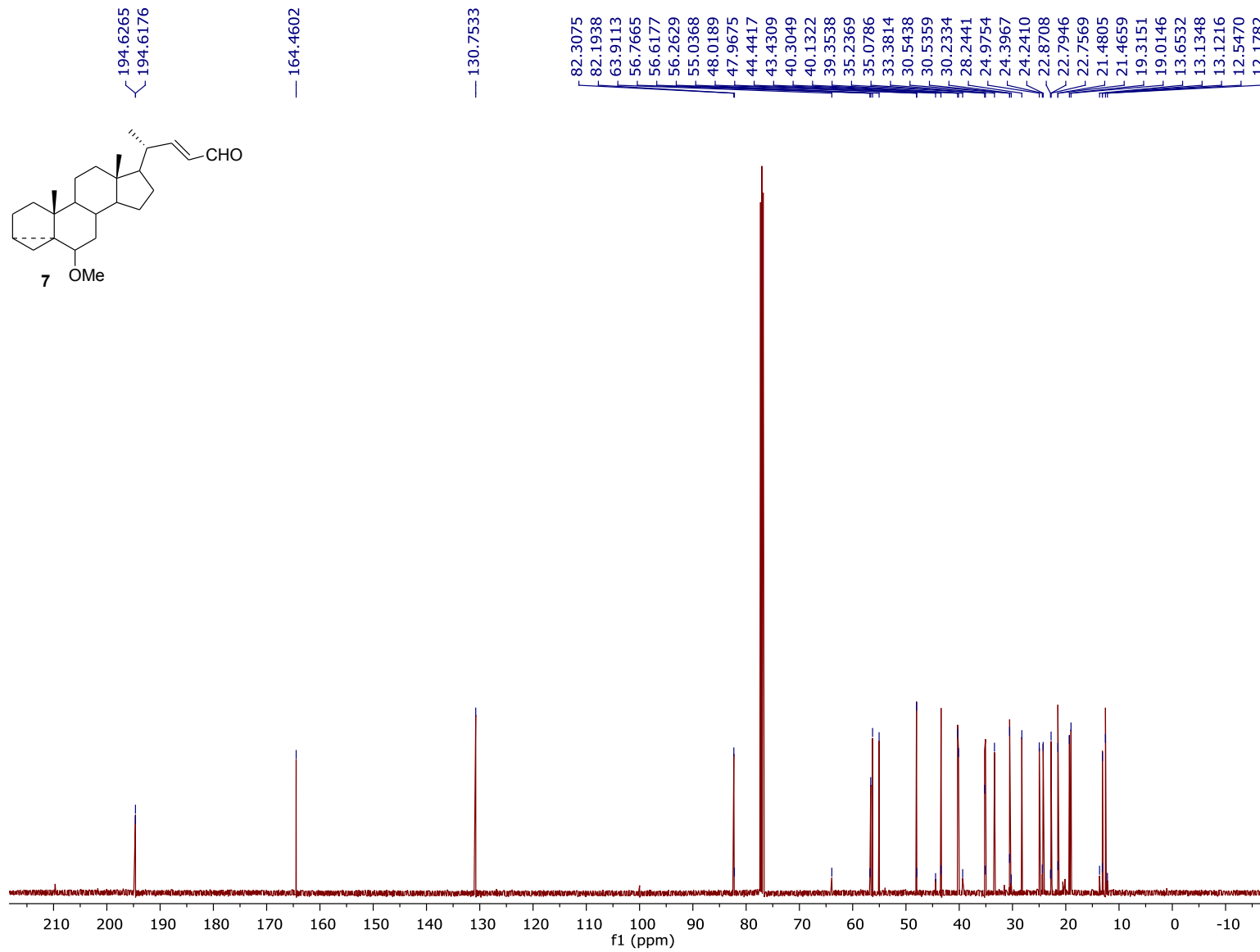
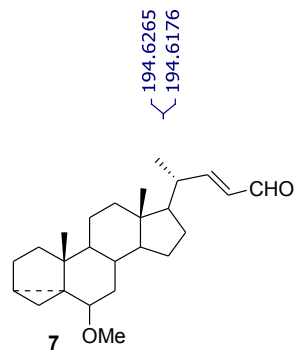


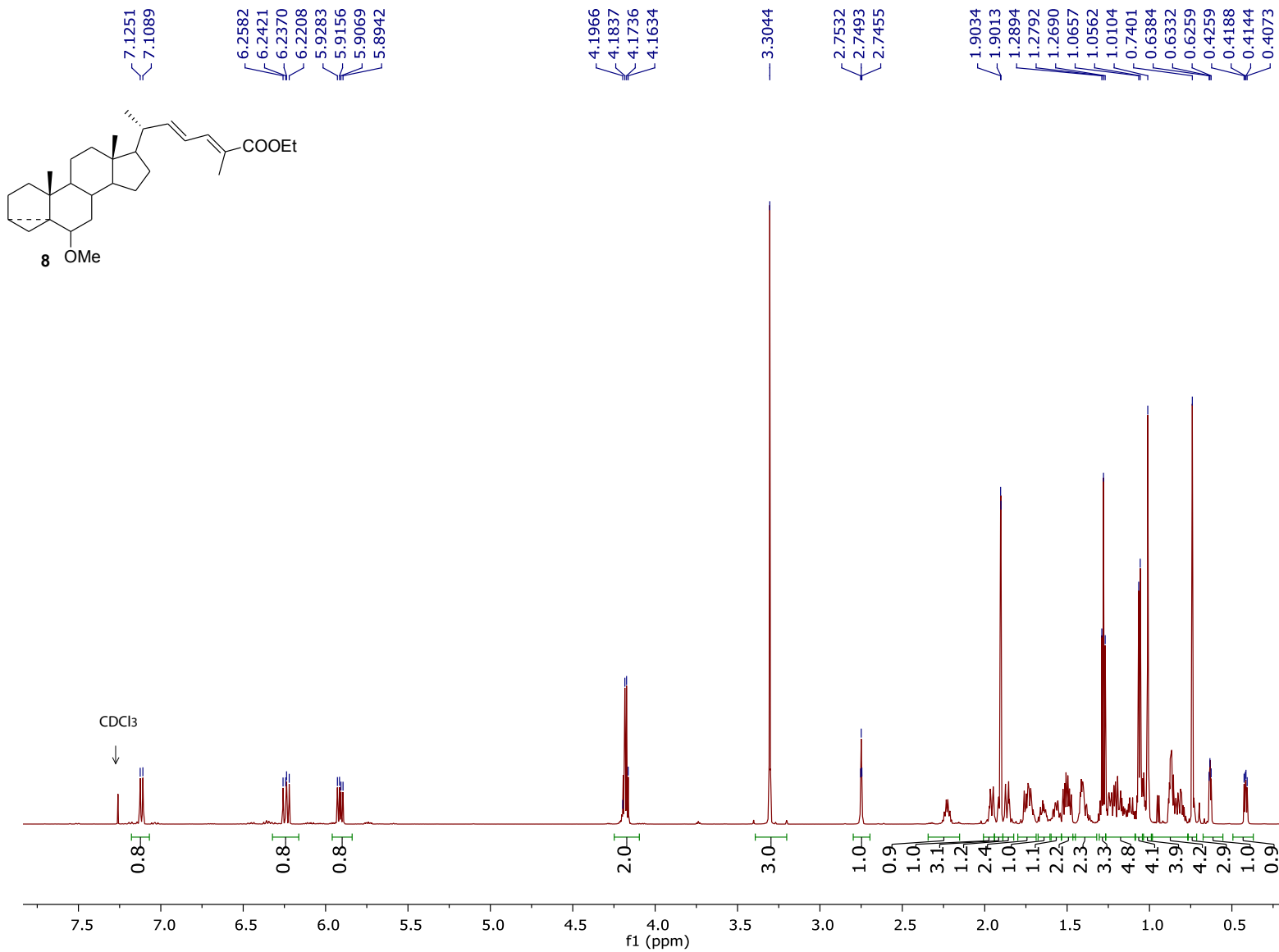


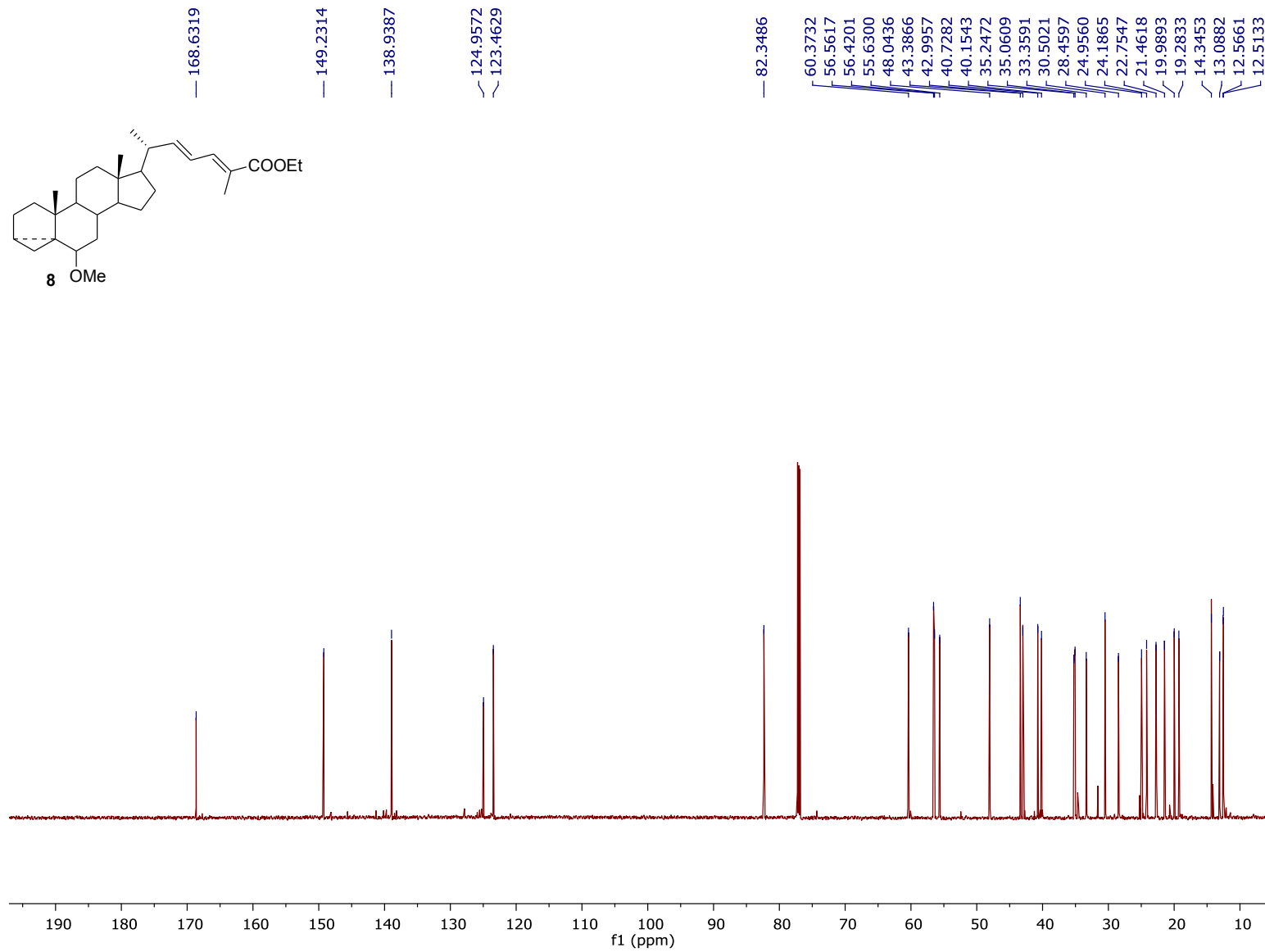


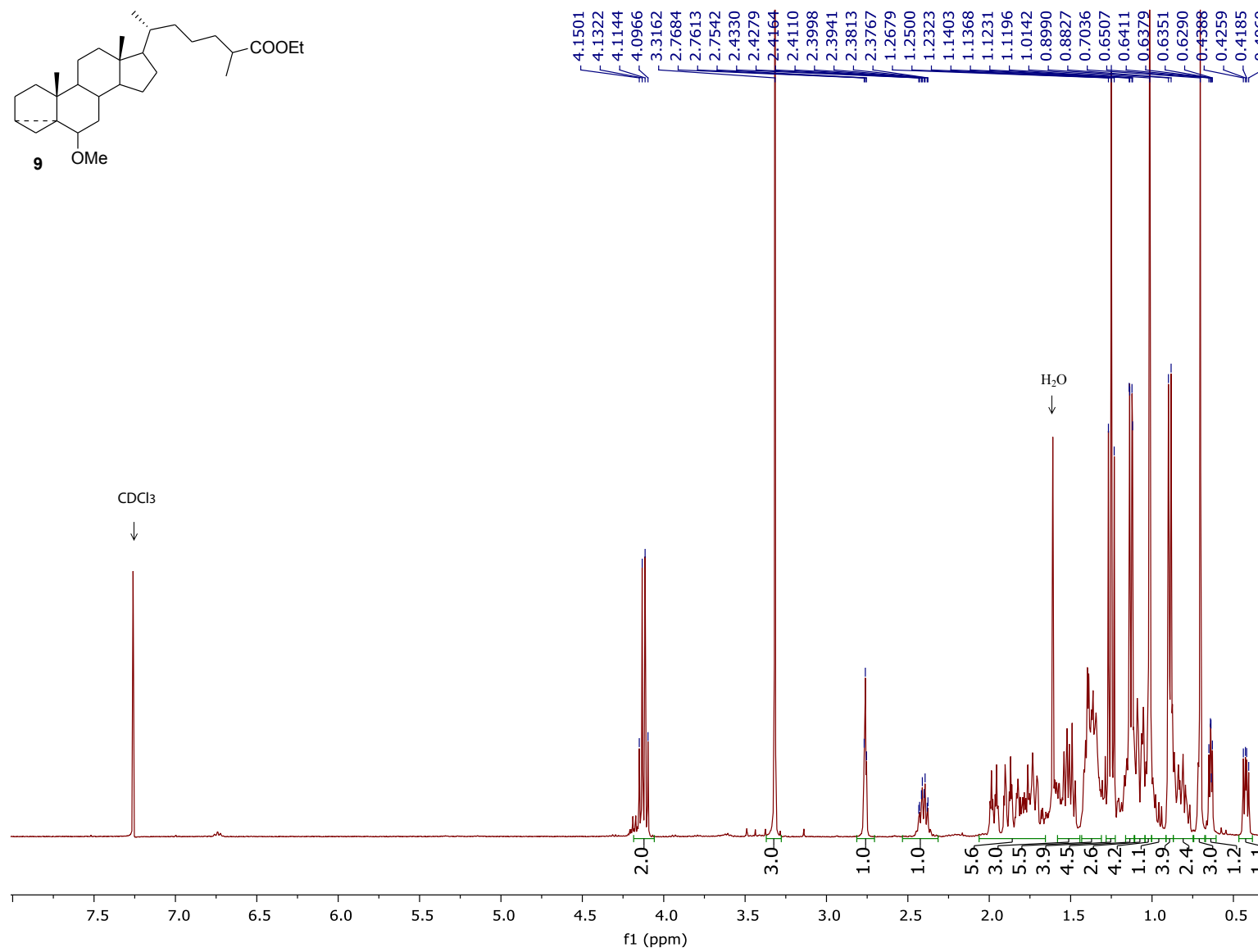
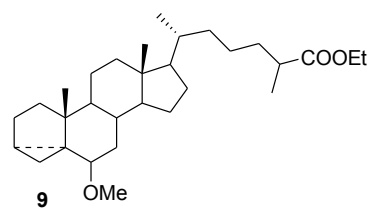


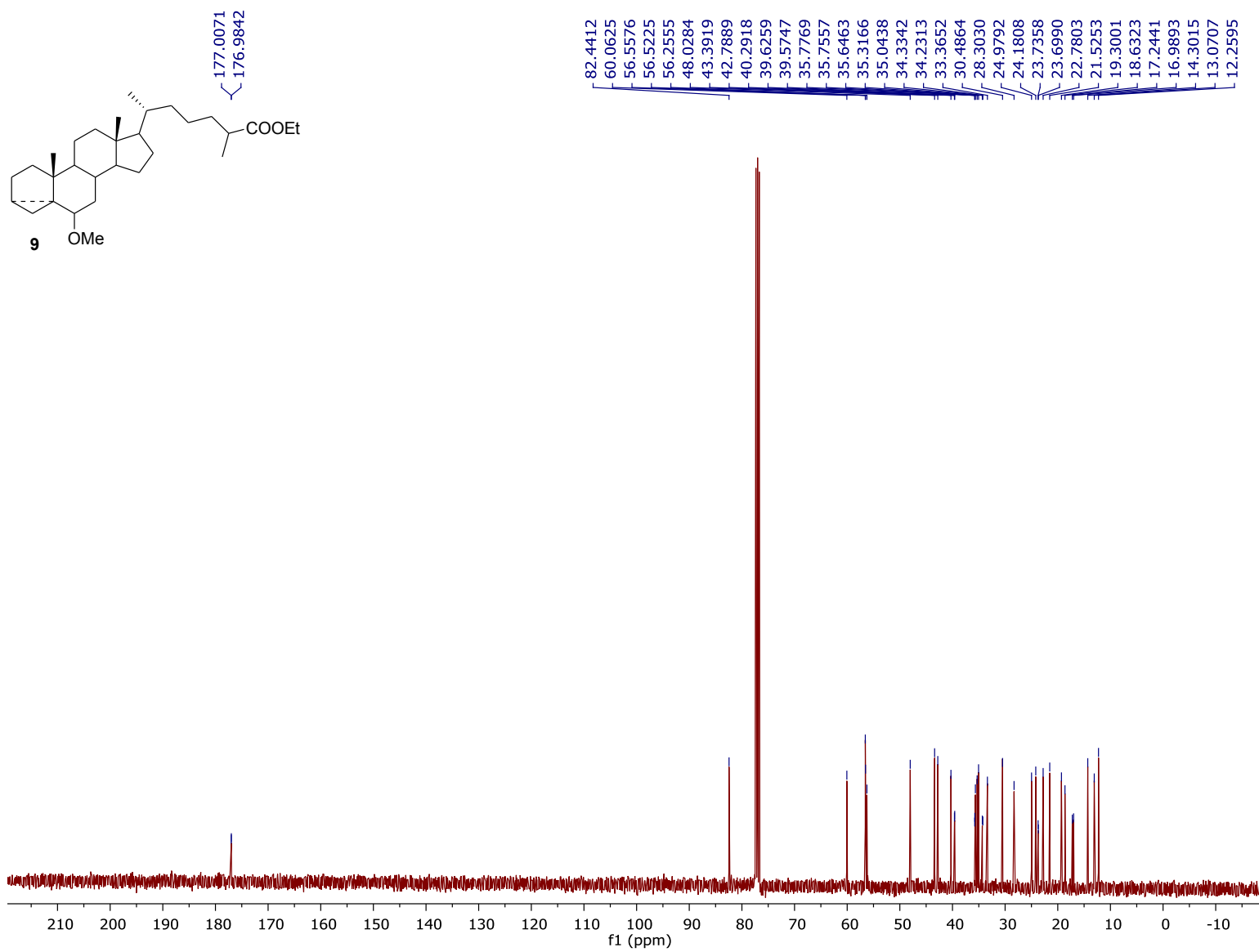


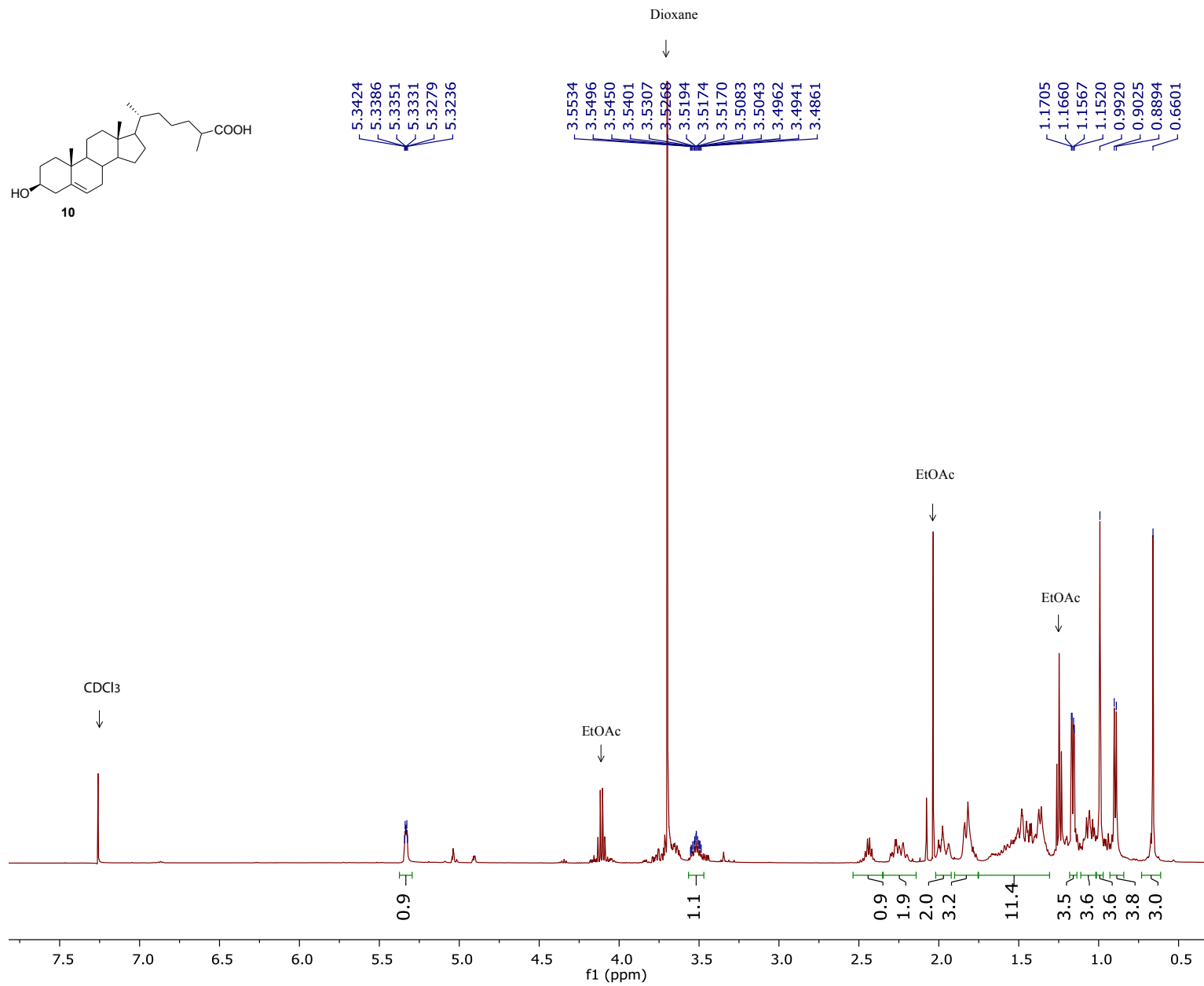
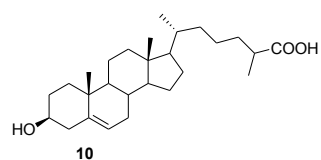


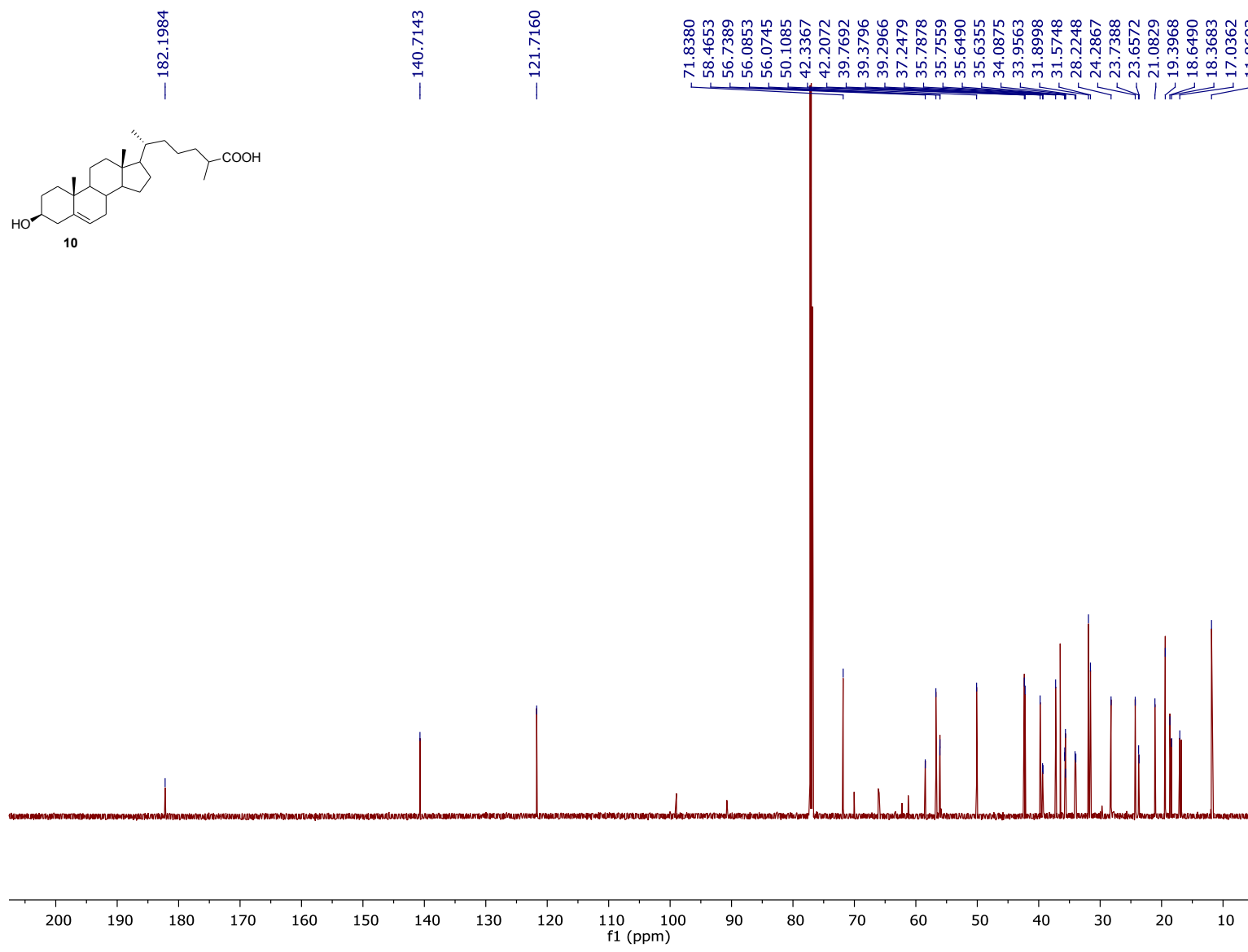


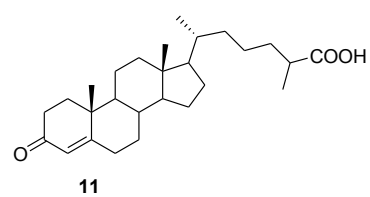












— 5.7257

